Electronic Supplementary Information

Electrolessly-Tin-Plated Sulfur Nanocomposite for Practical Lean-Electrolyte Lithium–Sulfur Cells with a High-Loading Sulfur Cathode

Chui-Yi Kung,[1] Sheng-Heng Chung[1,2,*]

[1] Department of Materials Science and Engineering, National Cheng Kung University, No. 1, University Road, Tainan City 70101

[2] Hierarchical Green-Energy Materials Research Center, National Cheng Kung University, No. 1, University Road, Tainan City 70101

[*]Corresponding authors: SHChung@gs.ncku.edu.tw (S.-H. Chung)

Experimental

Electrolessly-Tin-Plated Sulfur Nanocomposite: A tin-plated sulfur nanocomposite was synthesized *via* the electroless-plating method, in which tin metal was autocatalytically deposited onto the surface of sulfur particles. Specifically, pure sulfur powder (sulfur, 99.5%, Alfa Aesar) was first added to a sensitization solution and sensitized for 1 h with continuous stirring for catalytic surface formation. The sensitization solution comprised 0.1 g of stannous chloride ($SnCl_2$, 98%, Alfa Aesar) with 0.4 mL of hydrochloric acid (Honeywell Fluka) in 10 mL of deionized water. Subsequently, the sensitized sulfur powder was added to an activation solution and activated for 1 h with continuous stirring for the deposition of palladium as a catalytic seed. The activation solution included 0.0025 g of palladium chloride ($PdCl_2$, 99.9%, UniRegion Bio-Tech) and 0.025 mL of hydrochloric acid. Afterward, the activated sulfur powder was added to a mixed oxidizing/reducing solution and stirred for 15, 30, 45, 60, and 120 min to conduct the autocatalytic reaction at 80°C and 90°C and explore the optimal electroless-plating conditions. Stannous chloride (0.28–1.1 g; $SnCl_2$ 98%, Alfa Aesar) and 1.55 g of tri-sodium citrate dihydrate ($Na_3C_6H_5O_7 \cdot 2H_2O$, 99.0%, Alfa Aesar) were dissolved in 15 mL of deionized water to form the oxidizing solution with 0.10–0.40 M metal salt, and 1.05 g of sodium hypophosphite ($NaH_2PO_2 \cdot H_2O$, Alfa Aesar) was dissolved in 15 mL of deionized water to form the reducing solution. The tin-plated sulfur nanocomposites with tin contents of 15, 25, and 35 wt% were named Sn-15%, Sn-25%, and Sn-35%, respectively.

Material Characterization: Scanning electron microscopy and energy-dispersive X-ray spectroscopy analyses were performed using a scanning electron microscope with an energy-

dispersive X-ray spectroscope (SEM/EDS, JSM-7001F, JEOL). Transmission electron microscopy and energy-dispersive X-ray spectroscopy analyses were performed using a transmission electron microscope with an energy-dispersive X-ray spectroscope (TEM/EDS, JEM-2100F, JEOL). The specific surface area and pore-size distribution analysis of the current collector and the samples were measured using a high vacuum adsorption analyzer (Autosorb-iQ, Anton Paar) and analyzed using the Brunauer–Emmett–Teller (BET), Horvath–Kawazoe (HK), density functional theory (DFT), and Barrett–Joyner–Halenda (BJH) methods. Thermogravimetric analysis was performed using a thermogravimetric analyzer (TGA 4000, PerkinElmer) at a heating rate of 5 °C min^{-1} from 50°C to 500°C. Different electrolessly-tin-plated sulfur nanocomposite samples were subjected to thermogravimetric analysis (Fig. 1b–1d and S1). The polysulfide-trapped tin-plating shell retrieved from the tin-plated sulfur nanocomposite and the tin powder in the tin/sulfur composite were subjected to thermogravimetric analysis from 50°C to 600°C (Fig. 4g). Elemental analysis was performed using an elemental analyzer (Elementar Unicube). True density analysis was performed using a gas pycnometer (Ultrapyc 5000 Micro, Anton Paar), with the nitrogen gas at 18 psi and 25°C. X-ray diffraction analysis was performed using an X-ray diffractometer (D8 DISCOVER, Bruker), with the Cu Kα source operated at 40 kV and 30 mA, and 2θ values of 10°–80°. Ultraviolet–visible absorption spectroscopy was performed on a spectrophotometer (U4100, Hitachi), with wavelengths of 280–600 nm. XPS spectra was performed using X-ray photoelectron spectroscope (XPS, PHI 5000 VersaProbe III, Ulvac-Phi) with the Al Kα source to analyze the tin-plated sulfur nanocomposite Sn-25% before and after measurement.

Electrochemical and Electrocatalyst Characterization: Electrochemical impedance analysis and cyclic voltammetry analysis were performed using an electrochemical working station (VMP 300, Biologic) at frequencies of 0.1 MHz to 10 mHz with an alternating current amplitude of 0.2 mV and at increasing scanning rates of 0.02, 0.03, and 0.04 mV s^{-1}, with a voltage window of 1.6–2.8 V. The rate-dependent cyclic voltammetry data were collected to study the lithium-ion diffusion coefficient ($coefficient_{(Li\text{-}ion)}$) calculated according to the Randles–Ševčík equation: $i_{peak} = 268{,}600 \times e^{1.5} \times area \times coefficient_{(Li\text{-}ion)}^{0.5} \times concentration_{(Li\text{-}ion)} \times rate^{0.5}$. Accordingly, we studied the effect of the potential sweeping rate (*rate*) on the peak current (i_{peak}) under a fixed number of electrons (*e*), cathode area (*area*), and lithium-ion concentration of the electrolyte ($concentration_{(Li\text{-}ion)}$). Polysulfide adsorption analyses were performed using a 0.0025 M Li_2S_6 solution with a one-week resting period. The polysulfide adsorption capacities of sulfur and the tin-plated sulfur nanocomposite were analyzed with a blank reference, pure sulfur powder, Sn-15%, Sn-25%, and Sn-35% (Fig. 2g and 2h). The polysulfide adsorption capacities of the tin-plated sulfur nanocomposite and the tin/sulfur composite were analyzed using Sn-25% and the tin/sulfur mixture with 25 wt% tin (Fig. 4f). The sulfide nucleation analysis was performed with Sn-0%, Sn-15%, Sn-25%, and Sn-35%. The tin-plated sulfur nanocomposites and reference sulfur samples were drop-cast on the commercial carbon-paper current collector. The resulting cathodes were assembled in a cell with a high sulfur loading of 6 mg cm^{-2} and low electrolyte-to-sulfur ratio of 7 μL mg^{-1}. Subsequently, the sulfide nucleation analysis first galvanostatically discharged the cells with a constant current of 0.50 mA until the voltage reached 2.10 V, followed by a potentiostatic discharge at 2.09 V until the current density decreased to 2.4 μA. The sulfide dissolution analysis was performed with the same cell configuration with Sn-0%, Sn-15%, Sn-25%, and Sn-35% samples, while first galvanostatically discharging the cells with a constant current of 0.50 mA until

the voltage reached 1.60 V, followed by potentiostatic charging at 2.4 V until the current density decreased to 2.4 μA for lithium sulfide dissolution. The symmetric cell was prepared with 0.2 M Li_2S_6 and the tin-plated sulfur nanocomposites in the electrolyte and analyzed at 100 mV s^{-1} between −1.0 and 1.0 V.

Cell Performance: The tin-plated sulfur nanocomposites Sn-15%, Sn-25%, and Sn-35% were drop-cast on commercial carbon-paper current collectors (specific surface area of 80 m^2 g^{-1} before and after adding the active material) with tin contents of 15, 25, and 35 wt%, respectively, to form high-loading sulfur cathodes with 6 mg cm^{-2} (sulfur contents of 54, 50, and 45 wt%, respectively) and 10 mg cm^{-2} (58 wt%) sulfur. The sulfur content in parentheses includes the total electrode mass. The high-loading sulfur cathode was coupled with a lithium-metal counter/reference electrode, to which a polymeric separator was added to fabricate the lean-electrolyte lithium–sulfur cells with low electrolyte-to-sulfur ratios of 7, 6, 5, and 4 μL mg^{-1}. The electrolyte was prepared with 1.85 M lithium bis(trifluoromethanesulfonyl)imide (99.95%, Sigma-Aldrich) and 0.2 M lithium nitrate (99.98%, Alfa Aesar) in a 1,3-dioxolane (99.5%, Alfa Aesar)/1,2-dimethoxyethane (99+%, Alfa Aesar) mixture at a volumetric ratio of 40:55 (*i.e.*, 42% vs. 58%). The resulting lean-electrolyte cells were analyzed using a programable battery cycler (CT-4008-5V10mA, Neware) at room temperature to study the discharge–charge voltage profiles; cycling performances at C/10, C/5, C/3, and C/2 rates; and rate performance from C/20 to C/2 between 1.6 and 2.8 V for 200 cycles. A sulfur cathode was prepared as a reference. A tin/sulfur composite cathode was prepared through the mixing of 25 wt% tin and 75 wt% sulfur, after which the mixture was drop-cast on the same current collector used in the S+Sn-25% cell in Fig. 4.

Supporting Figures

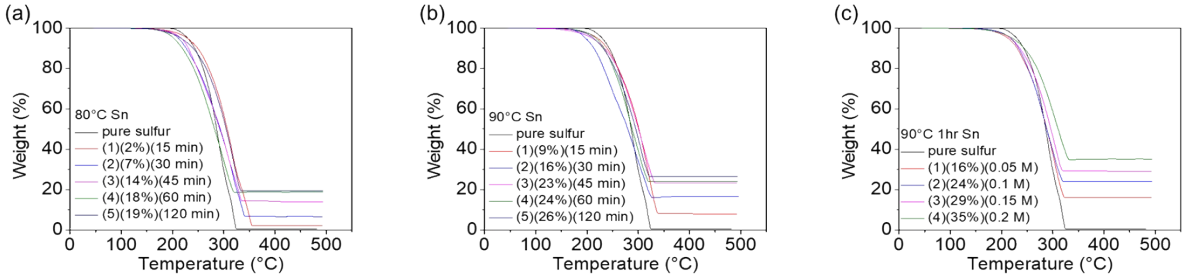

Fig. S1. Material characteristics. Thermogravimetric analysis of the tin-plated sulfur nanocomposites synthesized at (a) 80°C for different plating times (the numbers 1–5 in parentheses in Fig. S1a corresponds to the data points in Fig. 1a), (b) 90°C for different plating times (the numbers 1–5 in parentheses in Fig. S1b corresponds to the data points in Fig. 1b), and (c) 90°C for 1 h at different concentrations (the numbers 1–4 in parentheses in Fig. S1c corresponds to the data points in Fig. 1c).

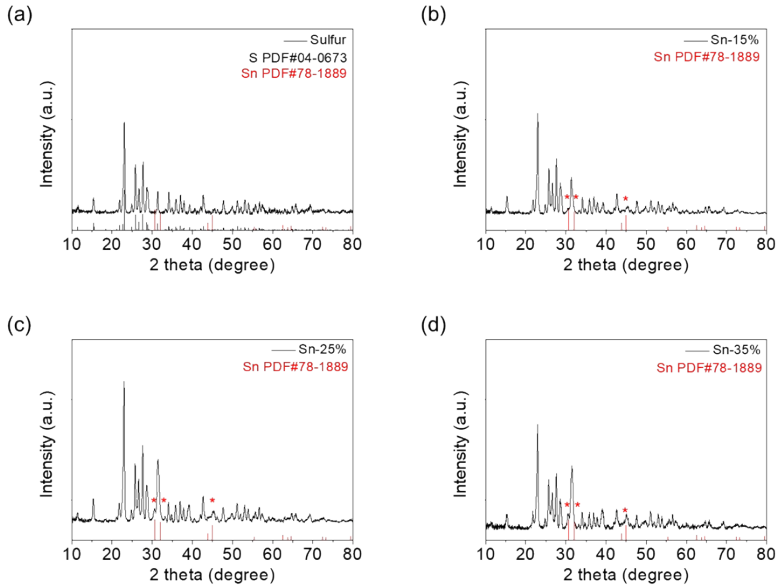

Fig. S2. Material characteristics. X-ray diffraction patterns of (a) sulfur and tin-plated sulfur nanocomposites: (b) Sn-15%, (c) Sn-25%, and (d) Sn-35%.

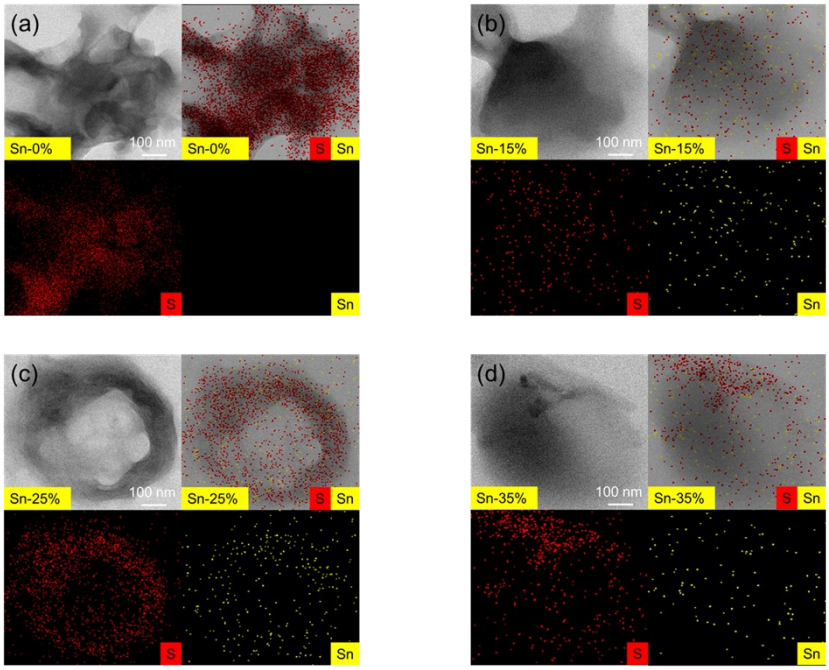

Fig. S3. Material characteristics. Transmission electron microscopy (TEM) analysis of (a) sulfur and tin-plated sulfur nanocomposites: (b) Sn-15%, (c) Sn-25%, and (d) Sn-35%.

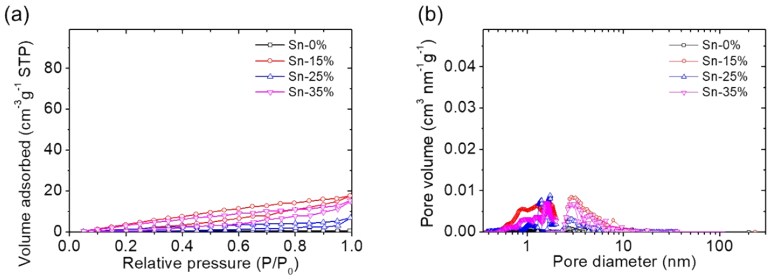

Fig. S4. Material characteristics. (a) nitrogen adsorption isotherms diagram of sulfur and tin-plated sulfur nanocomposites (b) pore-size distributions diagram of sulfur and tin-plated sulfur nanocomposites.

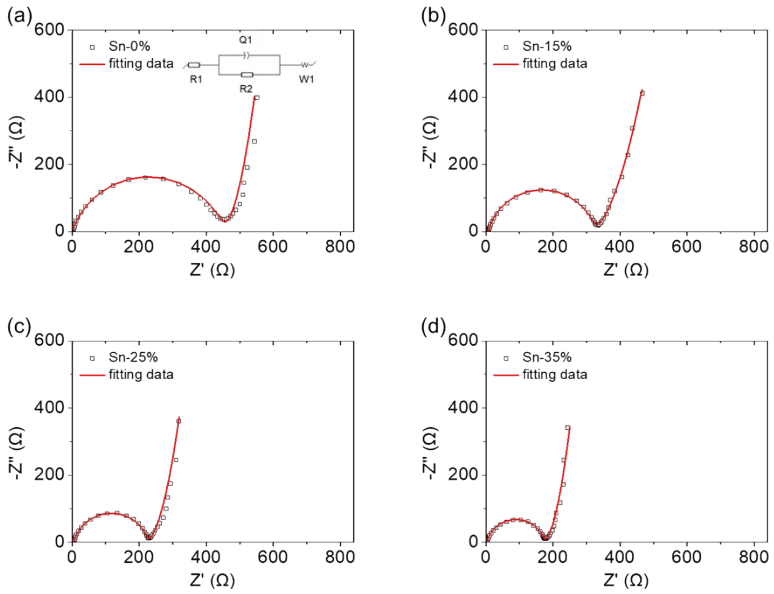

Fig. S5. Electrochemical and electrocatalytic characteristics. Electrochemical impedance spectra of uncycled (a) sulfur, (b) Sn-15%, (c) Sn-25%, and (d) Sn-35%. The experimental data and fitting data are shown as data points and fitting curves.

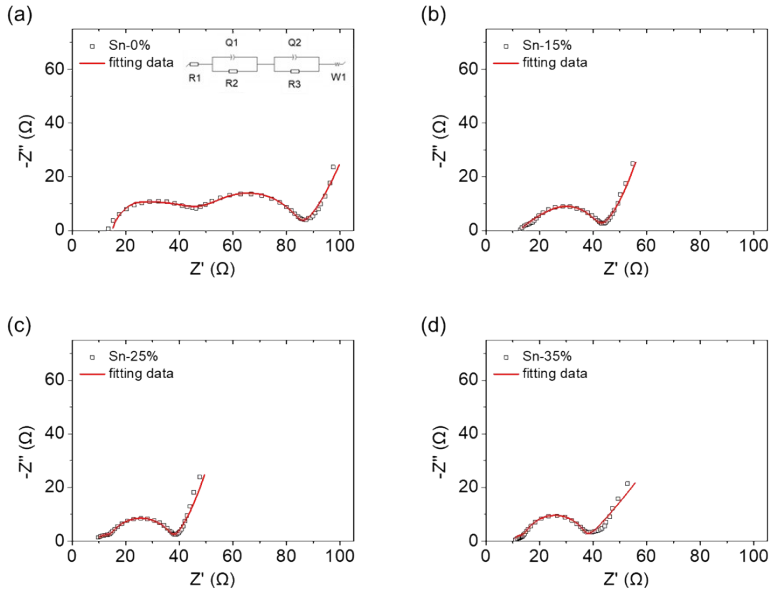

Fig. S6. Electrochemical and electrocatalytic characteristics. Electrochemical impedance spectra of cycled (a) sulfur, (b) Sn-15%, (c) Sn-25%, and (d) Sn-35%. The experimental data and fitting data are shown as data points and fitting curves.

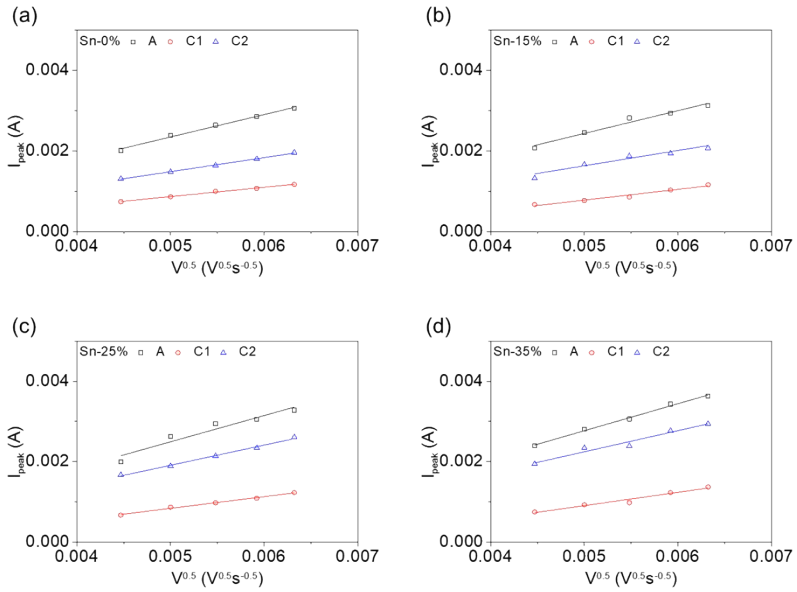

Fig. S7. Electrochemical and electrocatalytic characteristics. Lithium-ion diffusion coefficients of (a) sulfur, (b) Sn-15%, (c) Sn-25%, and (d) Sn-35%.

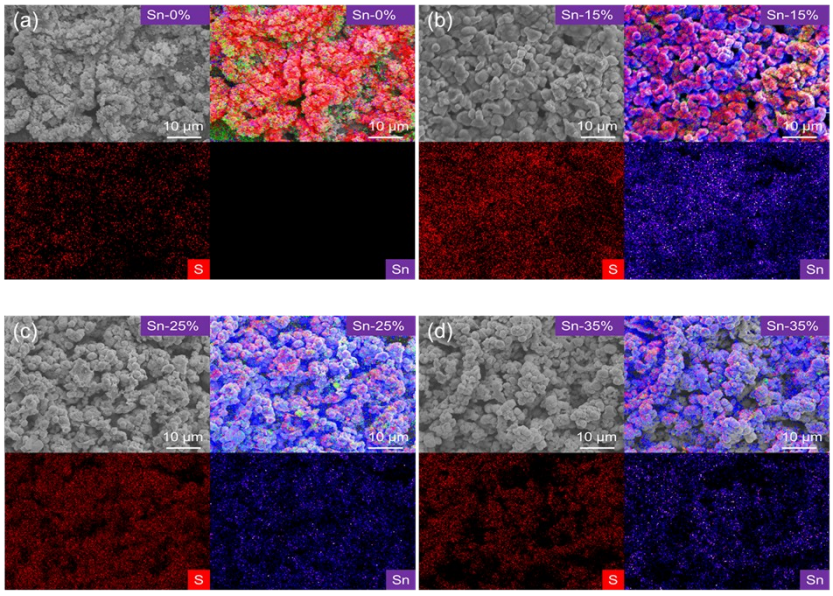

Fig. S8. Material characteristics. Scanning electron microscopy and energy-dispersive X-ray spectroscopy images of sulfur and tin-plated sulfur cathodes of cycled (a) Sn-0%, (b) Sn-15%, (c) Sn-25%, and (d) Sn-35%.

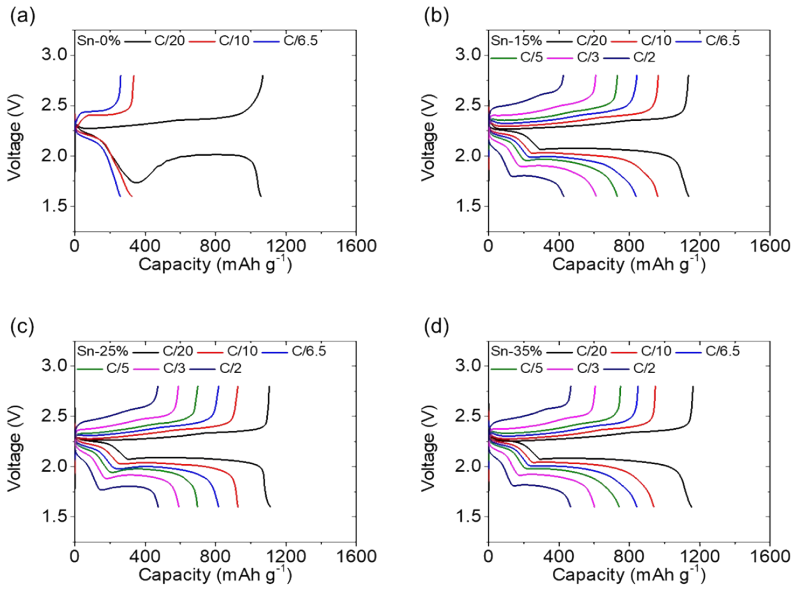

Fig. S9. Cell performance. Discharge–charge voltage profiles of (a) sulfur, (b) Sn-15%, (c) Sn-25%, and (d) Sn-35% at C/20 to C/2 rates.

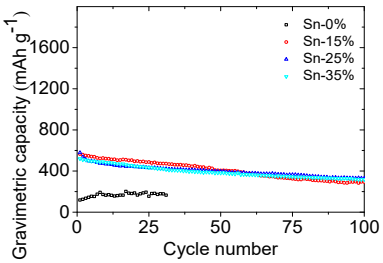

Fig. S10. Cell performance. Gravimetric capacity of sulfur, Sn-15%, Sn-25%, and Sn-35% at a C/10 rate for 100 cycles.

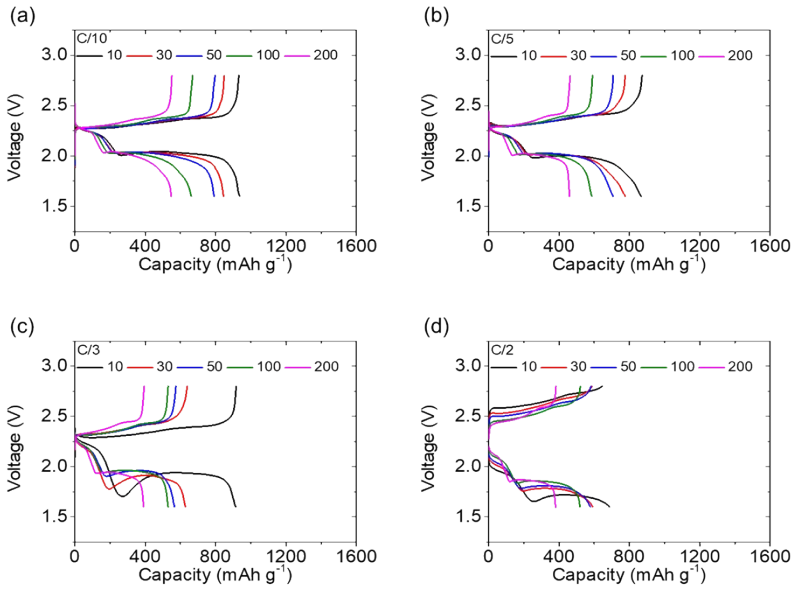

Fig. S11. Cell performance. Discharge–charge voltage profiles of the Sn-25% tin-plated sulfur nanocomposite at (a) C/10, (b) C/5, (c) C/3, and (d) C/2 rates for 200 cycles.

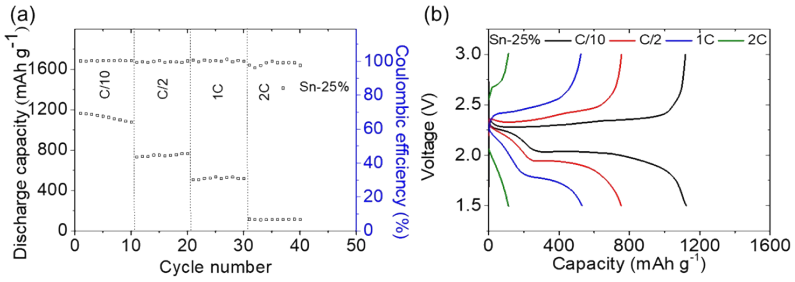

Fig. S12. Cell performance. (a) High rate performances and (b) discharge–charge voltage profiles of the Sn-25% tin-plated sulfur nanocomposite at C/10 to 2C.

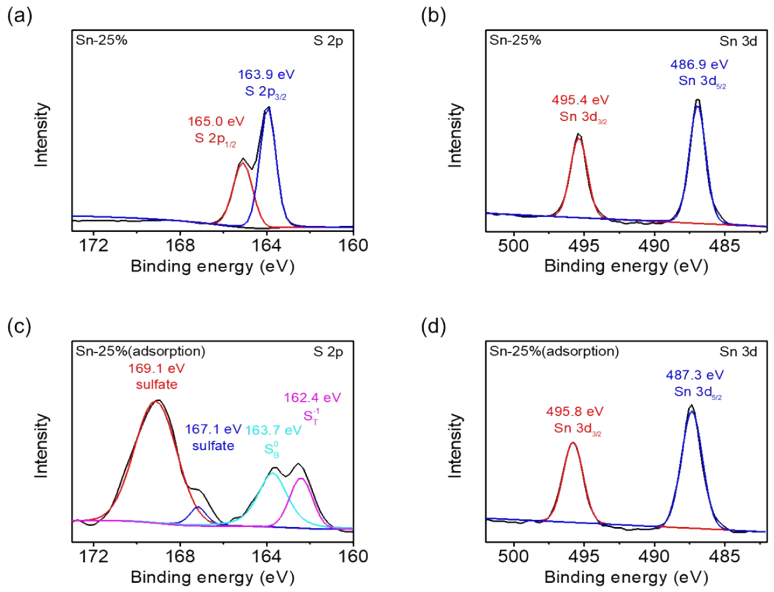

Fig. S13. Material characteristics. The XPS spectra of (a, b) the Sn-25% tin-plated sulfur nanocomposite and (c, d) the polysulfide-adsorbing Sn-25% tin-plated sulfur nanocomposite.

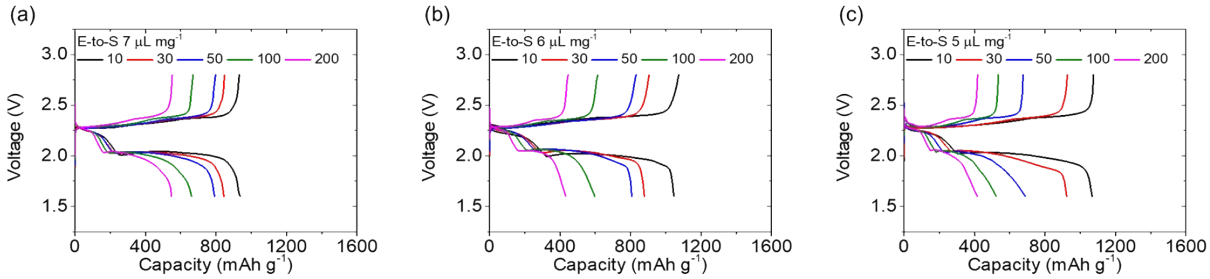

Fig. S14. Cell performance. Discharge–charge voltage profiles of the Sn-25% tin-plated sulfur nanocomposite at low electrolyte-to-sulfur ratios of (a) 7, (b) 6, and (c) 5 μL mg^{-1} for 200 cycles.

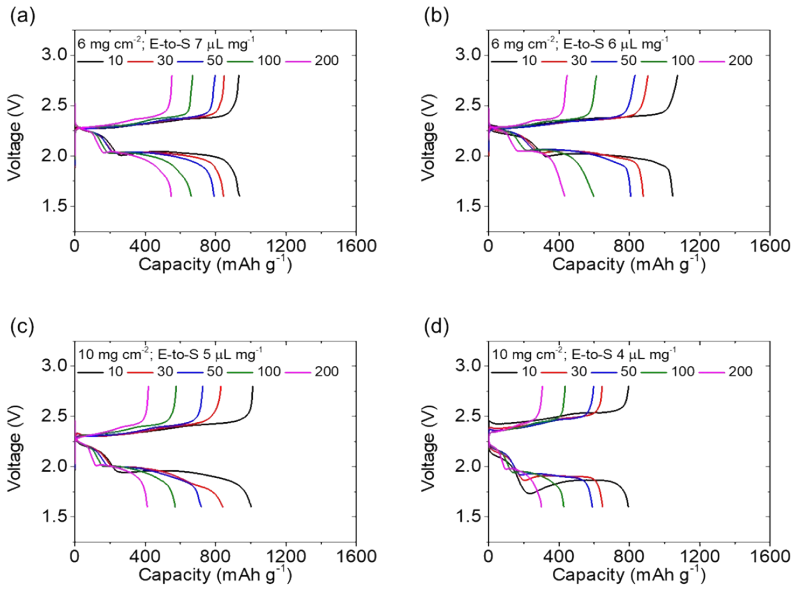

Fig. S15. Cell performance. Discharge–charge voltage profiles of the Sn-25% tin-plated sulfur nanocomposite with 6 mg cm^{-2} sulfur at low electrolyte-to-sulfur ratios of (a) 7 and (b) 6 µL mg^{-1} for 200 cycles and with 10 mg cm^{-2} sulfur at low electrolyte-to-sulfur ratios of (c) 5 and (d) 4 µL mg^{-1} for 200 cycles.

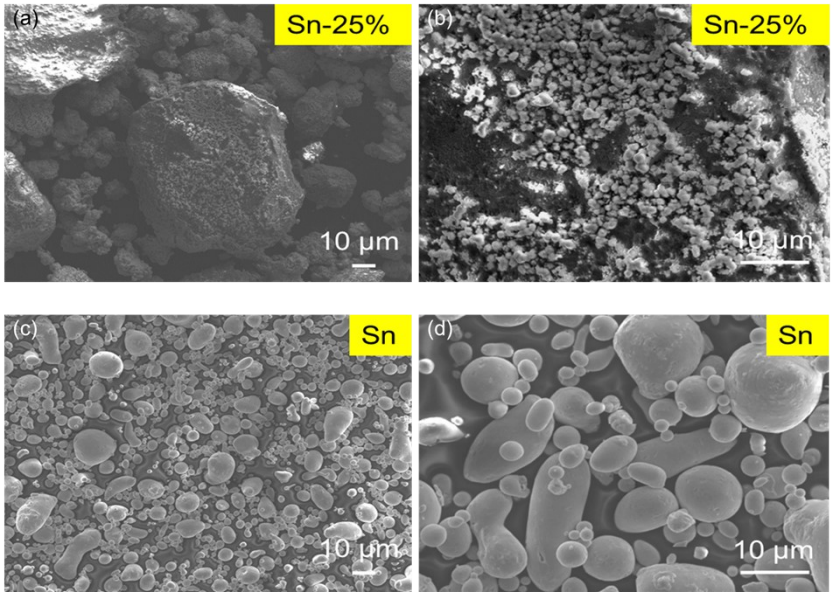

Fig. S16. Material characteristics. Scanning electron microscopy images of the tin particles of (a, b) the Sn-25% tin-plated sulfur nanocomposite and (c, d) the S+Sn-25% sulfur/tin composite.

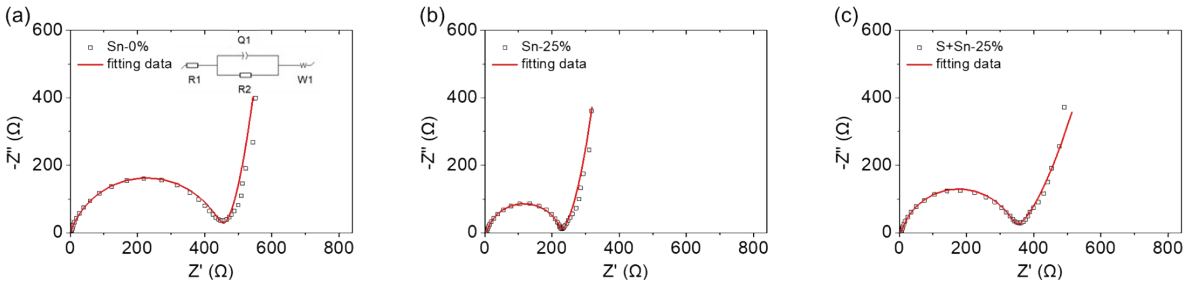

Fig. S17. Electrochemical characteristics. Electrochemical impedance spectra of uncycled (a) sulfur, (b) Sn-25% tin-plated sulfur nanocomposite, and (c) S+Sn-25% sulfur/tin composite.

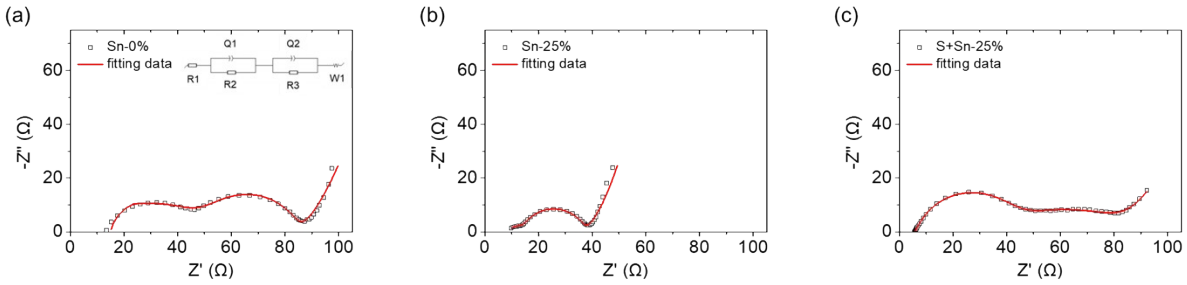

Fig. S18. Electrochemical characteristics. Electrochemical impedance spectra of cycled (a) sulfur, (b) Sn-25% tin-plated sulfur nanocomposite, and (c) S+Sn-25% sulfur/tin composite.

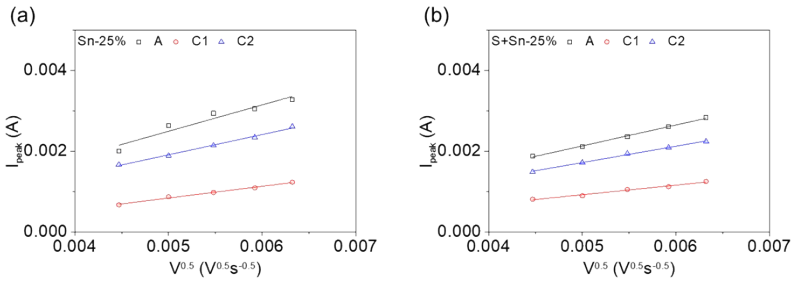

Fig. S19. Electrochemical characteristics. The lithium-ion diffusion coefficients of (a) the Sn-25% tin-plated sulfur nanocomposite and (b) the S+Sn-25% sulfur/tin composite.

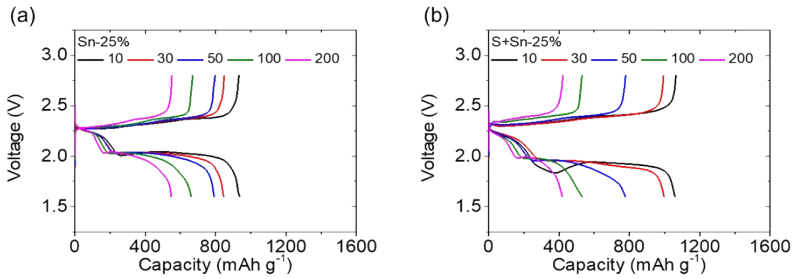

Fig. S20. Cell performance. Discharge–charge voltage profiles of (a) the Sn-25% tin-plated sulfur nanocomposite and (b) the S+Sn-25% sulfur/tin composite at a C/10 rate for 200 cycles.

Supporting Tables

Table S1. Material characteristics. Specific surface area and pore-size distributions analysis of sulfur and tin-plated sulfur nanocomposites.

	Sn-0%	Sn-15%	Sn-25%	Sn-35%
Surface Area ($m^2 g^{-1}$)	0.07	0.01	3.74	0.01
Total Pore Volume ($cm^3 g^{-1}$)	0.01	0.03	0.01	0.02

Table S2. Material characteristics. Thermogravimetric analysis, elemental analysis, energy-dispersive X-ray spectroscopy analysis, and true density analysis of sulfur and tin-plated sulfur nanocomposites.

EA	Sn-0%	Sn-15%	Sn-25%	Sn-35%
C%	0.0%	0.0%	0.0%	0.0%
H%	0.5%	0.3%	0.1%	0.1%
O%	0.0%	1.5%	0.6%	0.5%
S%	99.5%	85.3%	78.0%	67.9%
Sn%	0.0%	13.0%	21.4%	31.4%
EDS				
S%	100.0%	82.2%	75.4%	61.9%
Sn%	0.0%	17.8%	24.6%	38.1%
TDA				
true density ($g\ cm^{-3}$)	2.04	2.31	2.46	2.76
S%	100.0%	83.8%	76.3%	63.8%
Sn%	0.0%	16.2%	23.7%	36.2%
TGA	0.0%	16.4%	24.8%	35.9%
EA	0.0%	13.0%	21.4%	31.4%
EDS	0.0%	17.8%	24.6%	38.1%
TDA	0.0%	16.2%	23.7%	36.2%

Table S3. Electrochemical and electrocatalytic characteristics. The electrochemical impedance analysis results and lithium-ion diffusion coefficients of sulfur and tin-plated sulfur nanocomposites.

EIS (before cycling)	Sn-0%	Sn-15%	Sn-25%	Sn-35%
R_s (Ω)	3.3	6.8	5.1	2.8
R_{ct} (Ω)	436.7	316.4	224.2	172.7
EIS (after cycling)				
R_s (Ω)	13.4	12.6	9.2	10.6
R_{ct} (Ω)	54.7	21.0	23.5	22.7
R_{pf} (Ω)	30.2	9.2	4.3	4.0
CV				
A ($cm^2\ s^{-1}$)	1.5×10^{-7}	1.6×10^{-7}	2.1×10^{-7}	2.3×10^{-7}
C1 ($cm^2\ s^{-1}$)	2.7×10^{-8}	3.6×10^{-8}	4.3×10^{-8}	5.5×10^{-8}
C2 ($cm^2\ s^{-1}$)	6.2×10^{-8}	7.7×10^{-8}	1.3×10^{-7}	1.4×10^{-7}

Table S4. Development trend of the cell-design parameters and the resulting cell-performance values of recent lithium-sulfur battery with advanced sulfur-based composite cathodes.

Reference	Sulfur loading (mg cm^{-2})	E-to-S (μL mg^{-1})	Peak capacity (mA·h g^{-1})	Areal capacity (mA·h cm^{-2})	Energy density (mW·h cm^{-2})	E-to-C (μL mA·h^{-1})
R1	1.4	20	958	1.34	2.82	20.88
R2	2.0	20	1236	2.47	5.19	16.18
R3	3.7	20	1123	4.12	8.65	17.81
R4	4.2	10	1155	4.85	10.19	8.66
R5	1.6	18	966	1.50	3.14	18.63
R6	3.1	10	1150	3.57	7.49	8.70
R7	2.0	20	1210	2.42	5.08	16.53
R8	5.6	8	1035	5.80	12.17	7.73
R9	2.5	15	1252	3.13	6.57	11.98
R10	1.5	6	1398	2.10	4.40	4.29
R11	7.6	6	1073	8.20	17.22	5.59
R12	1.3	15	1089	1.42	2.97	13.77
R13	5.0	10	1254	6.27	13.17	7.97
R14	4.7	15	758	3.56	7.48	19.79
R15	5.0	5	923	4.62	9.69	5.42
R16	6.3	13	1100	6.93	14.55	11.82
R17	8.0	6	663	5.30	11.14	9.43
R18	6.8	20	1387	9.43	19.81	14.42
R19	10.0	10	822	8.22	17.26	12.17
R20	14.0	7	901	12.61	26.49	7.77
This Work	10	5	1143	11.43	24.00	4.37
	10	4	1066	10.66	22.39	3.75

Table S5. Electrochemical and electrocatalytic characteristics. The electrochemical impedance analysis results and lithium-ion diffusion coefficients of the Sn-25% tin-plated sulfur nanocomposite and the S+Sn-25% sulfur/tin composite.

EIS (before cycling)	Sn-25%	S+Sn-25%
R_s (Ω)	5.1	4.9
R_{ct} (Ω)	224.2	354.7
EIS (after cycling)		
R_s (Ω)	9.2	5.5
R_{ct} (Ω)	23.5	47.4
R_{pf} (Ω)	4.3	32.4
CV		
A ($cm^2\ s^{-1}$)	2.1×10^{-7}	1.3×10^{-7}
C1 ($cm^2\ s^{-1}$)	4.3×10^{-8}	2.8×10^{-8}
C2 ($cm^2\ s^{-1}$)	1.3×10^{-7}	8.3×10^{-8}

Supporting References

R1. C. Wang, H. Song, C. Yu, Z. Ullah, Z. Guan, R. Chu, Y. Zhang, L. Zhao, Q. Li and L. Liu, *J. Mater. Chem. A*, 2020, **8**, 3421–3430.

R2. Q. Shao, L. Xu, D. Guo, Y. Su and J. Chen, *J. Mater. Chem. A*, 2020, **8**, 23772–23783.

R3. D. Wang, Q. Cao, B. Jing, X. Wang, T. Huang, P. Zeng, S. Jiang, Q. Zhang and J. Sun, *Chem. Eng. J.*, 2020, **399**, 125723.

R4. R. Xiao, T. Yu, S. Yang, K. Chen, Z. Li, Z. Liu, T. Hu, G. Hu, J. Li, H.-M. Cheng, Z. Sun and F. Li, *Energy Stor. Mater*., 2022, **51**, 890–899.

R5. S. Majumder, M. Shao, Y. Deng and G. Chen, *J. Power Sources*, 2019, **431**, 93–104.

R6. W. Jing, J. Zu, K. Zou, X. Dai, Y. Song, J. Sun, Y. Chen, Q. Tan and Y. Liu, *J. Colloid. Interface Sci.*, 2023, **635**, 32–42.

R7. Z. Du, X. Chen, W. Hu, C. Chuang, S. Xie, A. Hu, W. Yan, X. Kong, X. Wu, H. Ji and L. J. Wan, *J. Am. Chem. Soc.*, 2019, **141**, 3977–3985.

R8. Y. Qiu, L. Fan, M. Wang, X. Yin, X. Wu, X. Sun, D. Tian, B. Guan, D. Tang and N. Zhang, *ACS Nano*, 2020, **14**, 16105–16113.

R9. J. Liu, S. H. Xiao, Z. Zhang, Y. Chen, Y. Xiang, X. Liu, J. S. Chen and P. Chen, *Nanoscale*, 2020, **12**, 5114–5124.

R10. H. Wang, D. Wei, J. Zheng, B. Zhang, M. Ling, Y. Hou and C. Liang, *ACS Appl. Energy Mater.*, 2020, **3**, 11893–11899.

R11. X. Sun, D. Tian, X. Song, B. Jiang, C. Zhao, Y. Zhang, L. Yang, L. Fan, X. Yin and N. Zhang, *Nano Energy*, 2022, **95**, 106979.

R12. N. Li, K. Chen, S. Chen, F. Wang, D. Wang, F. Gan, X. He and Y. Huang, *Carbon*, 2019, **149**, 564–571.

R13. C. Ma, Y. Zhang, Y. Feng, N. Wang, L. Zhou, C. Liang, L. Chen, Y. Lai, X. Ji, C. Yan and W. Wei, *Adv. Mater.*, 2021, **33**, e2100171.

R14. Z. Su, M. Chen, Y. Pan, Y. Liu, H. Xu, Y. Zhang and D. Long, *J. Mater. Chem. A*, 2020, **8**, 24117–24127.

R15. Y. Tsao, H. Gong, S. Chen, G. Chen, Y. Liu, T. Z. Gao, Y. Cui and Z. Bao, *Adv. Energy Mater.*, 2021, **11**, 2101449.

R16. V. Marangon, D. Di Lecce, F. Orsatti, D. J. L. Brett, P. R. Shearing and J. Hassoun, *Sustain. Energy Fuels*, 2020, **4**, 2907–2923.

R17. Z. Yu, B. Wang, X. Liao, K. Zhao, Z. Yang, F. Xia, C. Sun, Z. Wang, C. Fan, J. Zhang and Y. Wang, *Adv. Energy Mater.*, 2020, **10**, 2000907.

R18. Y. Wei, Y. Wang, X. Zhang, B. Wang, Q. Wang, N. Wu, Y. Zhang and H. Wu, *ACS Appl. Mater. Interfaces*, 2020, **12**, 35058–35070.

R19. C.-S. Cheng and S.-H. Chung, *Batter. Supercaps*, 2022, **5**, e202100323.

R20. C.-S. Cheng and S.-H. Chung, *Chem. Eng. J.*, 2022, **429**, 132257.